Journal of Global Positioning Systems (2009)
Vol.8, No.2 :135-147
doi:10.5081/jgps.8.2.135

Journal of Global Positioning Systems
2009
© CPGPS

Performance Evaluation of Combined L1/L5 Kalman Filter-Based Tracking versus Standalone L1/L5 Tracking in Challenging Environments

Dina Reda Salem, Cillian O'Driscoll and Gérard Lachapelle
Position, Location And Navigation (PLAN) Group, Department of Geomatics Engineering
Schulich School of Engineering, University of Calgary

Abstract

The ever-increasing demand on GPS to perform in challenging environments is the main motivation behind this research. With the existence of these challenging environments, more research is directed towards enhancing the tracking capabilities. Several solutions have been proposed to enable high sensitivity tracking using only one signal. However, new GPS signals are now available, in addition to the conventional L1 signal. Being transmitted from the same space vehicle through the same environment, the errors between these signals are correlated. Hence, an increase in tracking sensitivity can be achieved by combining two or more of these signals. This paper proposes the idea of combining the L1 and L5 signals using one Kalman filter, where the correlator outputs of the two signals are used to estimate the tracking errors. The performance of this combined Kalman filter is compared to a similar Kalman filter that is used separately for tracking each of the two signals. The performance of both filters is compared in environments suffering urban canyon multipath, moderate ionospheric errors, in addition to a motion model of a typical vehicle. The combined Kalman filter is shown to outperform the separate Kalman filter, both in the tracking errors and in the filter statistics.

Keywords: L5 signal, signals combination, combined Kalman filter tracking, standalone Kalman filter tracking

1 Introduction

Previous research has been done to combine two signals for tracking: Gernot et al (2008) discussed the idea of combining the L1 C/A code and the L2C signals at the discriminator level, where the outputs of the discriminators are applied to least square filter to estimate the discriminator errors and the ionospheric parameters.

The choice of the L5 signal over the other new signals has its reasons. The L5 signal is specially designed for emergency and safety of life applications; hence, it is located in the Aeronautical Radio Navigation Service (ARNS) band, and allocated the carrier frequency of 1176.45 MHz. Though the L5 lower carrier frequency causes it to be more vulnerable to the ionospheric errors, the existence of the pilot channel and the 6 dB stronger power of the L5 signal (Ward et al 2006), together with the enhanced code properties (IS-GPS-2006 2006), makes it attractive to use it together with the L1 C/A code signal.

The Kalman filter and its variants have been frequently used for L1 C/A signal tracking. As for the L5 signal, Mongrédien et al (2008) have tested the Kalman filter on the L5 signal and compared it with other tracking techniques. Megahed et al (2009) introduced the idea of combining the L1 C/A code signal and the L5 signal in one Kalman filter. A Kalman filter model, capable of the combined tracking of the L1 C/A and L5 signals, was fully developed and demonstrated in ibid. The state space consisted of the tracking errors of both the L1 and the L5 signals, including the code phase errors, the carrier phase and frequency errors, and the driving carrier acceleration force, together with their effective amplitudes. The Kalman filter was specially designed to enhance the observability and to allow the combination of the two signals. The process noises were modified and their mathematical models are shown.

This paper presents further enhancements made to the model presented in the Megahed (2009). To analyze the performance of the combined Kalman filter tracking thoroughly, a comparison is performed between the separate Kalman filter tracking of the L1 and the L5 signals, and the combined Kalman filter tracking. The primary difference between the separate and the combined Kalman filters is the availability of more information in the combined Kalman filter from both signals. The combined Kalman filter has the advantage of using the correlator outputs of both signals to estimate the

tracking errors; therefore, it operates in a collaborative manner. The advantages also appear in environments that suffer multipath, where the L5 can be of a great help to the L1 signal. Further advantages appear in moderate to strong ionospheric errors, where the L1 signal can help the L5 signal. Several environments are simulated using a Spirent GSS7700 simulator since no satellites are currently transmitting the L5 signal (with the exception of SVN 49, which is transmitting a non-standard signal).

The environments under consideration include a static vehicle in an urban canyon multipath environment with moderate ionospheric activity, and another user motion model that included high acceleration values for a vehicle and a sudden change in direction under moderate levels of ionospheric activity. Results show that the combined Kalman filter outperforms the separate Kalman filter in the tests conducted.

The paper is structured as follows. It starts with an overview on the signal and system model used. The relationship between the two signals of interest is outlined in section 2. Section 3 explains the iterated extended Kalman filter used in implementing the two filters compared in this paper. It then illustrates the separate Kalman filter model used for tracking each of the two signals, and for evaluating the combined Kalman filter, follwed by a demonstration of the combined Kalman filter. The section also discusses the process noise spectral densities in each of the filters utilized. Section 4 shows the test setup followed by a description of different simulated environments and the results obtained from each model. The paper finally concludes with a summary and the future work in section 5.

2 Signals And Systems Models

The signals under consideration are the L1 C/A signal and the L5 signal. The signal models are given by equations (1) and (2).

For the L1 signal:

$$S_{L1}(t) = \sqrt{P_{L1}}.D_{L1}(t).C_{L1}(t)\cos(2\pi f_{L1}t + \varphi_{L1}) \qquad (1)$$

For the L5 signal (Mongredien et al 2006):

$$S_{L5}(t) = \sqrt{2P_{L5}}.\begin{bmatrix} D_{L5}(t).C_{data}(t).NH_{10}(t).\cos(2\pi f_{L5}t + \varphi_{L5}) \\ +C_{pilot}(t).NH_{20}(t).\sin(2\pi f_{L5}t + \varphi_{L5}) \end{bmatrix} \qquad (2)$$

where:

P_{L1}, P_{L5}	Total received power for the L1 and L5 signal respectively
D_{L1}, D_{L5}	Navigation data bits for the L1 and L5 signal respectively
C_{L1}	L1 C/A code
C_{data},C_{pilot}	Pseudo-Random Noise (PRN) codes for the data and the pilot channels respectively of the L5 signal.
NH_{10}, NH_{20}	The 10 and 20 bit Neuman-Hoffman codes applied to the data and the pilot channels respectively of the L5 signal.
f_{L1}, f_{L5}	L1 and L5 carrier frequency respectively.
ϕ_{L1},ϕ_{L5}	L1 and L5 carrier phase respectively.

After the code and the carrier wipe-off of the two signals, the resulting correlator outputs are given in equations (3) and (4). For the current paper, only the L5 pilot signal is used to completely benefit from the absence of any data bits.

$$\begin{aligned} IP_{L1} &= A_{L1}.N_{L1}.D_{L1}.R(\delta\tau_{L1}).\cos(\overline{\delta\phi_{L1}}) \\ QP_{L1} &= A_{L1}.N_{L1}.D_{L1}.R(\delta\tau_{L1}).\sin(\overline{\delta\phi_{L1}}) \end{aligned} \qquad (3)$$

$$\begin{aligned} IP_{L5} &= A_{L5}.N_{L5}.R(\delta\tau_{L5}).\cos(\overline{\delta\phi_{L5}}) \\ QP_{L5} &= A_{L5}.N_{L5}.R(\delta\tau_{L5}).\sin(\overline{\delta\phi_{L5}}) \end{aligned} \qquad (4)$$

and

$$A_{L1} = \sqrt{P_{L1}}\frac{\sin(\pi\delta f_{L1}T)}{\pi\delta f_{L1}T}, A_{L5} = \frac{\sqrt{P_{L5}}}{2}\frac{\sin(\pi\delta f_{L5}T)}{\pi\delta f_{L5}T} \qquad (5)$$

where:

A_{L1}, A_{L5}	The effective amplitude of the L1 and the L5 pilot signals.
N_{L1},N_{L5}	The number of accumulated samples for both the L1 and the L5 signals.
$R(\delta\tau_{L1}),R(\delta\tau_{L5})$	The correlation of the filtered incoming code with the local generated code for the L1 and the L5 signals respectively.
T	The coherent integration time.
$\delta\tau_{L1},\delta\tau_{L5}$	The L1 and the L5 local code phase error in units of chips.
$\delta f_{L1},\delta f_{L5}$	The L1 and the L5 local carrier frequency error in units of rad/s.
$\overline{\delta\varphi_{L1}},\overline{\delta\varphi_{L5}}$	The L1 and the L5 average local carrier phase error over the integration interval in units of rad.

The average phase errors can be expanded as (Psiaki & Jung 2002):

$$\delta\varphi = \delta\varphi_0 + \delta f_0 \frac{T}{2} + \alpha_0 \frac{T^2}{6} \quad (6)$$

where α_0. is the phase acceleration in units of rad/s^2. The subscript zero indicates the value at the start of the integration.

The early and late correlators for the two signals have the same parameters, each with early-late spacing set to one chip.

The prompt, early and late correlator outputs of both signals are then fed to the Kalman filter. The output of the Kalman filter contains the updates for the numerically controlled oscillator (NCO). Note that the combination of the two signals is done after acquisition, bit synchronization and frequency lock have been achieved.

3 Kalman Filter

Each of the two Kalman filter models that will be discussed in the paper follow the Kalman filter structure that has been used extensively in the literature (Petovello & Lachapelle (2006), Psiaki & Jung (2002) and Mongrédien et al (2008)). The Kalman filter generally constitutes of two models:

1) The state dynamic model that describes the dynamics of a continuous time system model,

$$\dot{x}(t) = F(t)x(t) + G(t)w(t) \quad (7)$$

where:

x	States of dynamic system
F	Coefficient matrix describing the dynamics of the system
G	Shaping matrix for the white noise input
w	Random forcing function, zero-mean white Gaussian noise.

2) The measurement model which includes the set of observations *z* available to estimate the states *x*. The state vector *x* is known to relate to the observation vector *z* as:

$$z_k = H_k x_k + v_k \quad (8)$$

where: z_k is the measurement vector, H_k is the design matrix, v_k is the measurement noise vector.

Each of the two filters under comparison are iterated extended Kalman filters (Table I), due to the non-linear nature of the measurement models used.

The table includes two steps that must be performed: 1) discretization of the dynamic matrix, 2) linearization of the measurement model. The details of these two steps can be found in Megahed et al (2009).

This structure of the Kalman filter is used for the two cases under consideration: the separate Kalman filter and the combined Kalman filter tracking. To enable a fair comparison between the two filters, they are required to follow exactly the same steps in the software receiver.

Fig. 1 shows the flowchart of the software receiver developed. It starts with the L1 and the L5 acquisition and bit synchronization, and then proceeds to the frequency tracking, and then the phase tracking of each signal. Up to that point, each of the two signals is dealt with separately. After phase lock is achieved, the receiver either proceeds to the separate Kalman filter tracking for each of the two signals, or the combined Kalman filter tracking.

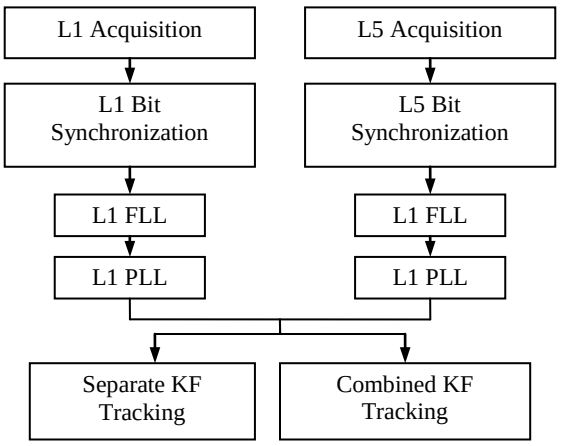

Fig. 1: Flowchart of separate and combined Kalman filters

To ensure a fair comparison, the dynamic model for the states is the same for the two filters. Further details will be presented in the following sections.

The next two sections will describe the two elements of comparison:

1) The separate Kalman filter tracking, in which each of the two signals is tracked separately.

2) The combined Kalman filter tracking, the main contribution of the paper.

Table I : Iterated Extended Kalman filter model	
Continuous Time System Model	$\dot{x}(t) = F(t)x(t) + G(t)w(t)$ $w(t) \sim N(0, Q(t))$
Nonlinear Measurement Model	$z_k = h_k(x_k(t)) + v_k$ $v_k \sim N(0, R_k)$
Discrete Time System Model	$x_k = \Phi_{k-1}x_{k-1} + w_{k-1}$ $w_k \sim N(0, Q_k)$
Linearized Measurement Model	$z_k = H_k x_k + v_k$ $v_k \sim N(0, R_k)$
Prediction Step	$\hat{x}_k(-) = \Phi_{k-1}\hat{x}_{k-1}(+)$ $P_k(-) = \Phi_{k-1}P_{k-1}(+)\Phi_{k-1}^T + Q_{k-1}$
Kalman Gain Matrix	$\overline{K}_k = P_k(-)H_k^T[H_k P_k(-)H_k^T + R_k]^{-1}$
Update Step	$\hat{x}_k(+) = \hat{x}_k(-) + \overline{K}_k[z_k - H_k\hat{x}_k(-)]$ $P_k(+) = [I - \overline{K}_k H_k]P_k(-)$

where:

x	State vector
F(t)	Coefficient matrix describing the dynamics of the system
G(t)	Shaping matrix for the white noise input
w	Random forcing function, zero-mean white Gaussian noise.
Φ_k	State transition matrix
z_k	Measurement vector
h_k	Nonlinear design matrix
H_k	Linearized Design matrix
v_k	Measurement noise
Q(t)	Process noise spectral density matrix
R_k	Covariance matrix for the measurement noise
P_k	State Covariance Matrix
K_k	Kalman Gain

3.1 Separate Kalman Filter

The separate Kalman filter-tracking model adopted is the one introduced by Psiaki & Jung (2002), and modified by Petovello & Lachapelle (2006).

Fig. 2 shows the steps for tracking each of the L1 and the L5 signals. For the L1 signal, the incoming signal undergoes a carrier wipe-off, followed by a code wipe-off. The output of this stage is then applied to the Kalman filter to extract the tracking errors, and use these to update the NCOs.

The L5 signal undergoes the exact same steps, a carrier wipe-off, followed by a code wipe-off. An extra step is required to wipe-off the NH codes. Since the pilot L5 signal only is used, the NH20 codes are required to be wiped-off. Then the steps proceed similar to those for the L1 signal.

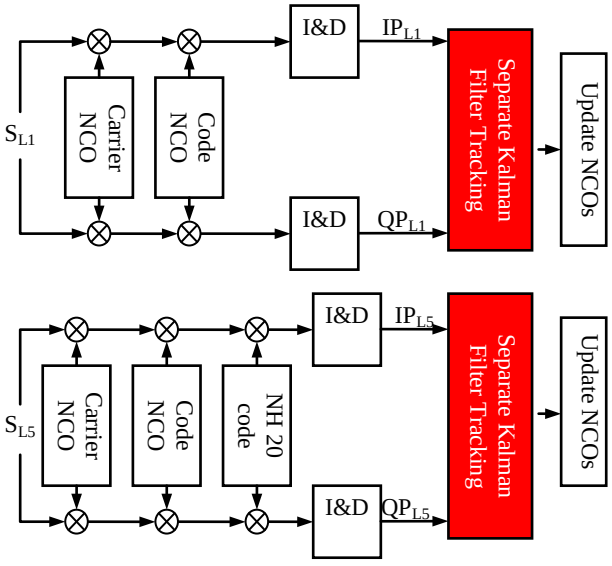

Fig. 2: Separate Kalman filter Tracking

State Space Model:

The states to be estimated in single signal tracking are: the amplitude of the signal, the code phase error, the carrier phase error, the frequency error, and the carrier acceleration error. The carrier acceleration process noise accounts for the signal dynamics. The amplitude is

modelled as a random walk, and its process noise is expected to absorb the signal level variations. The code phase error is estimated from the carrier frequency error, with a two component process noise, w_{τ_1} and $\beta_1 w_{\phi_{0_1}}$. The random walk component w_{τ_1} accounts for any ionospheric error divergence between the code phase and carrier frequency, and the multipath. The carrier frequency and phase process noises account for the oscillator jitter effects.

The states to be estimated and the corresponding state space equations can be written as:

$$\begin{aligned} x_{L1} &= \begin{pmatrix} A_1 & \delta\tau_1 & \delta\phi_{01} & \delta f_{01} & \alpha_{01} \end{pmatrix}^T \\ x_{L5} &= \begin{pmatrix} A_5 & \delta\tau_5 & \delta\phi_{05} & \delta f_{05} & \alpha_{05} \end{pmatrix}^T \end{aligned} \quad (9)$$

where: *x* indicates the states to be estimated for the subscripted signal.

$$\frac{d}{dt}\begin{pmatrix} A_1 \\ \delta\tau_1 \\ \delta\phi_{0_1} \\ \delta f_{0_1} \\ \alpha_{0_1} \end{pmatrix} = \begin{pmatrix} 0 & 0 & 0 & 0 & 0 \\ 0 & 0 & 0 & \beta_1 & 0 \\ 0 & 0 & 0 & 1 & 0 \\ 0 & 0 & 0 & 0 & 1 \\ 0 & 0 & 0 & 0 & 0 \end{pmatrix} \begin{pmatrix} A_1 \\ \delta\tau_1 \\ \delta\phi_{0_1} \\ \delta f_{0_1} \\ \alpha_{0_1} \end{pmatrix} \quad (10)$$

$$+ \begin{pmatrix} 1 & 0 & 0 & 0 & 0 \\ 0 & 1 & \beta_1 & 0 & 0 \\ 0 & 0 & 1 & 0 & 0 \\ 0 & 0 & 0 & 1 & 0 \\ 0 & 0 & 0 & 0 & 1 \end{pmatrix} \begin{pmatrix} w_{A_1} \\ w_{\tau_1} \\ w_{\phi_{0_1}} \\ w_{f_{01}} \\ w_{\alpha_{01}} \end{pmatrix}$$

where: β converts units of radians into units of chips for the subscripted signal and *w* is the process noise of the subscripted quantity.

Measurement Model:

For each signal, the observations are formed from the six correlator outputs available; the inphase and quadraphase prompt, early, and late (IP, QP, IE, QE, IL, QL) correlators. These correlators are then used to estimate the state parameters shown in equation (9).

The *z* vector can thus be written as:

$$\begin{aligned} z_{L1} &= \begin{pmatrix} IP_{L1} & IE_{L1} & IL_{L1} & QP_{L1} & QE_{L1} & QL_{L1} \end{pmatrix}^T \\ z_{L5} &= \begin{pmatrix} IP_{L5} & IE_{L5} & IL_{L5} & QP_{L5} & QE_{L5} & QL_{L5} \end{pmatrix}^T \end{aligned} \quad (11)$$

Each of these correlator outputs carry the tracking information required to be estimated as shown in their representation in equations (3) and (4). However, these two equations reveal the non-linearity in the measurement model, which is why an additional step has to be added for the linearization. The details of the linearization step is shown in Megahed et al (2009).

3.2 Combined Kalman Filter

The combined Kalman filter was introduced by Megahed et al (2009). It makes use of the correlator outputs of both the L1 and the pilot L5 signals and applies them to a single Kalman filter to extract the tracking errors for each. The software receiver follows similar steps to that for the separate Kalman filter tracking. As shown in Fig. 3, first each of the two signals undergoes carrier and code wipe-off. The output of this stage, both the L1 and the L5 correlator outputs, is then applied to one Kalman filter instead of using two separate Kalman filters.

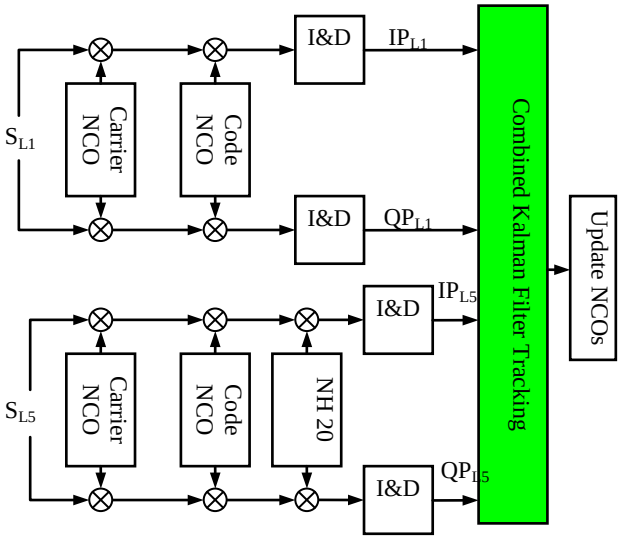

Fig. 3: Combined Kalman filter tracking

State Space Model:

The states to be estimated, discussed in the previous section can be written as:

$$x = \begin{pmatrix} A_1 & \delta\tau_1 & \delta\phi_{01} & A_5 & \delta\tau_5 & \delta\phi_{0_5} & \delta f_{05} & \alpha_{05} \end{pmatrix}^T \quad (12)$$

To ensure a fair comparison, the same dynamic model assumption is used for the combined filter. The L5 carrier phase acceleration noise is the driving force for the filter. It accounts for the L5 signal dynamics. The L5 carrier frequency and phase errors accounts for the oscillator jitters. The L1 carrier phase error is estimated from the L5 carrier frequency error. Note that a random walk noise was also added to the L1 carrier phase model to account for any divergence between the L1 carrier phase and the L5 carrier frequency. The value of this tuning parameter is determined by simulations. The L1 code phase error is estimated from the scaled L5 carrier frequency. A random walk component is added to the L1 code phase error to account for the L1 code and the L5 carrier divergence. The state space model is shown in equation (13).

$$\frac{d}{dt}\begin{pmatrix} A_1 \\ \delta\tau_1 \\ \delta\phi_{0_1} \\ A_5 \\ \delta\tau_5 \\ \delta\phi_{0_5} \\ \delta f_{0_5} \\ \alpha_{0_5} \end{pmatrix} = \left(\begin{array}{ccc|ccc|cc} 0 & 0 & 0 & 0 & 0 & 0 & 0 & 0 \\ 0 & 0 & 0 & 0 & 0 & 0 & \beta_1 \frac{f_{c,L1}}{f_{c,L5}} & 0 \\ 0 & 0 & 0 & 0 & 0 & 0 & \frac{f_{c,L1}}{f_{c,L5}} & 0 \\ \hline 0 & 0 & 0 & 0 & 0 & 0 & 0 & 0 \\ 0 & 0 & 0 & 0 & 0 & 0 & \beta_5 & 0 \\ 0 & 0 & 0 & 0 & 0 & 0 & 1 & 0 \\ 0 & 0 & 0 & 0 & 0 & 0 & 0 & 1 \\ 0 & 0 & 0 & 0 & 0 & 0 & 0 & 0 \end{array}\right) \begin{pmatrix} A_1 \\ \delta\tau_1 \\ \delta\phi_{0_1} \\ A_5 \\ \delta\tau_5 \\ \delta\phi_{0_5} \\ \delta f_{0_5} \\ \alpha_{0_5} \end{pmatrix} +$$

$$\left(\begin{array}{ccc|ccc|cc} 1 & 0 & 0 & 0 & 0 & 0 & 0 & 0 \\ 0 & 1 & 0 & 0 & 0 & \beta_1 \frac{f_{c,L1}}{f_{c,L5}} & 0 & 0 \\ 0 & 0 & 1 & 0 & 0 & \frac{f_{c,L1}}{f_{c,L5}} & 0 & 0 \\ \hline 0 & 0 & 0 & 1 & 0 & 0 & 0 & 0 \\ 0 & 0 & 0 & 0 & 1 & \beta_5 & 0 & 0 \\ 0 & 0 & 0 & 0 & 0 & 1 & 0 & 0 \\ 0 & 0 & 0 & 0 & 0 & 0 & 1 & 0 \\ 0 & 0 & 0 & 0 & 0 & 0 & 0 & 1 \end{array}\right) \begin{pmatrix} w_{A_1} \\ w_{\tau_1} \\ w_{\phi_{0_1}} \\ w_{A_5} \\ w_{\tau_5} \\ w_{\phi_{0_5}} \\ w_{f_{0_5}} \\ w_{\alpha_{0_5}} \end{pmatrix} \tag{13}$$

where: β converts units of radians into units of chips for the subscripted signal and *w* is the process noise of the subscripted quantity.

Measurement Model:

The observations are formed from the six correlator outputs available for each signal; the inphase and quadraphase prompt, early, and late (IP, QP, IE, QE, IL, QL) correlators for each of the L1 and the L5 pilot channels, presented in equation. These correlators are used to estimate the state parameters shown in equation (12).

The *z* vector can thus be written as:

$$z = \begin{pmatrix} IP_{L1} & IE_{L1} & IL_{L1} & QP_{L1} & QE_{L1} & QL_{L1} \\ IP_{L5} & IE_{L5} & IL_{L5} & QP_{L5} & QE_{L5} & QL_{L5} \end{pmatrix}^T \tag{14}$$

In order to obtain the design matrix of the combined Kalman filter, the $\overline{\delta\phi_{L1}}$ has to be re-expanded in terms of the L5 frequency and phase acceleration as shown in equation (15).

$$\begin{aligned} \overline{\delta\varphi_{L1}} &= \frac{1}{T}\int_0^T \delta\varphi_{L1}(t)dt \\ &= \delta\varphi_{0,L1} + \delta f_{0,L5}\frac{T}{2}\times\frac{f_{c,L1}}{f_{c,L5}} + \alpha_{0,L5}\frac{T^2}{6}\times\frac{f_{c,L1}}{f_{c,L5}} \end{aligned} \tag{15}$$

3.3 Process Noise

The process noise is an important tuning factor that has to be adjusted fairly in the two elements of comparison. For the separate Kalman filter tracking, we have five process noise spectral densities for each of the L1 and the L5 signals, whereas for the combined Kalman filter we have eight process noise spectral densities.

Three main tuning parameters are taken into consideration:

- Amplitude standard deviation: accounts for the signal level variations
- Code Carrier Divergence: accounts for the code carrier divergence due to ionospheric errors and multipath
- Line of Sight Spectral Density: that is the driving force for the filter

The other two process noises are the carrier phase and frequency; these are tuned according the oscillator used in the front-end receiver.

The combined Kalman filter tuning parameters are similar to those of the separate Kalman filter where in this case five tuning parameters are dealt with: the amplitude standard deviation of both the L1 and the L5 signals; the code carrier divergence of both; and the line of sight spectral density. To insure a fair comparison between the filters, the values used are the same, except for the L1 code phase process noise in the case of the combined Kalman filter. That value had to be modified to tune the combined Kalman filter to give the same code phase error estimates as the separate Kalman filter case.

Table II and Table III show the process noise spectral densities for both separate and the combined Kalman filter respectively.

Table II: Separate Kalman filter parameters

Process noise	Spectral density
A_s (dB/s/√Hz)	1
$\delta\tau_s$ (m/s /√Hz)	0. 1
$\delta\phi_s$ (cycles/s /√Hz)	$(2\pi f_s).\sqrt{(h_0/2)}$
δf_s (Hz/s /√Hz)	$(2\pi f_s).\sqrt{(2\pi^2 h_{-2})}$
α_s (m/s^3/√Hz)	5

where:

- The subscript *s* refers to the signal of interest.

- h_0, h_{-2} are the white noise and integrated frequency noise parameters for the OCXO oscillator used.

Table III Combined Kalman filter parameters

Process noise	Spectral density
A_{L1} (dB/s/√Hz)	1
$\delta\tau_{L1}$ (m/s/√Hz)	1
$\delta\phi_{L1}$. (cycles/s/√Hz)	0.6
A_{L5} (dB/s/√Hz)	1
$\delta\tau_{L5}$ (m/s/√Hz)	0.1
$\delta\phi_{L5}$ (cycles/s/√Hz)	$(2\pi f_s).\sqrt{(h_0/2)}$
δf_{L5} (Hz/s/√Hz)	$(2\pi f_s).\sqrt{((2\pi^2 h_{-2})}$
α_{L5} (m/s^3/√Hz)	5

4 TEST SETUP

In order to test and compare the two methods, a controllable environment is required to enable the simulation of different environments.

Although an L5 signal is now available, since a demo payload has been launched on SVN 49 in March 2009 (Inside GNSS 2009), the signal does not comply with the specifications of the IS-GPS-2006 (2006). Braasch et al (2009) and Meurer et al (2009) have highlighted several deviations of the demo L5 payload. First, the SVN 49 transmits only the dataless component, second: it is hardwired to transmit PRN 63. The third and of the most important to this paper's work, the transmitted power is much less than that in the specifications. Further more, as in *ibid*, the L5 signal power shows a significant elevation angle dependency, that ranges about 18 dB between the low and high elevation angles.

For these reasons, and in order to get correct performance measures using the original L5 signal specifications, a GSS7700 Spirant GPS signal simulator has been used. It has also the advantage of being able to simulate different environments for the L1 and the L5 signals. The simulated environments will be illustrated in the following sections. The RF output of the GSS7700 simulator is then passed to a National Instruments front-end which logs raw IF samples for each of the two signals, which are subsequently processed by the software receiver.

Fig. 4 shows the hardware setup. For a detailed description of the hardware setup, refer to Megahed et al (2009).

4.1 Simulation Environments

Two different environments were simulated using the Spirent GSS7700 simulator (Spirent 2006): The first is the land mobile multipath with an urban canyon multipath environment on a static vehicle, and the second is a dynamic user moving with a high acceleration for a vehicle and with sudden turns. The details of each simulation setup are as follows:

Test A: Urban Canyon Multipath

The first test is on a static vehicle operating in an urban canyon multipath environment.

- Static vehicle
- Land mobile multipath
- Urban canyon multipath environment

Several studies in the literature, e.g. Lachapelle et al (2003) and Hu et al (2005), have verified the matching of the simulated multipath environments using the Spirent signal simulator to the actual multipath environments.

The land mobile multipath model allows four categories for the signals determined by their arriving angles as shown in Fig. 5:

- Category A: Obstruction, that represents a visibility mask where all the signals below 5 degree of elevation are excluded.
- Category B: LOS only, signals that are unobstructed and not subject to any reflections. These signals suffer Rician fading only.
- Category C: LOS +Echoes, signals that are unobstructed but subject to reflections. The LOS signal suffers Rician fading, where the echoes suffer modified Rayleigh fading.
- Category D: Echoes only, these represent obstructed LOS signals that are present as reflections only, and they suffer modified Rayleigh fading.

For the test conducted, the satellite chosen must have both LOS and echoes. The signal being tracked during this test is that for PRN 5 (highlighted in Fig. 5). From the elevation and the azimuth angle of the satellite, it lies in the Category C, where it is simulated as LOS and echoes.

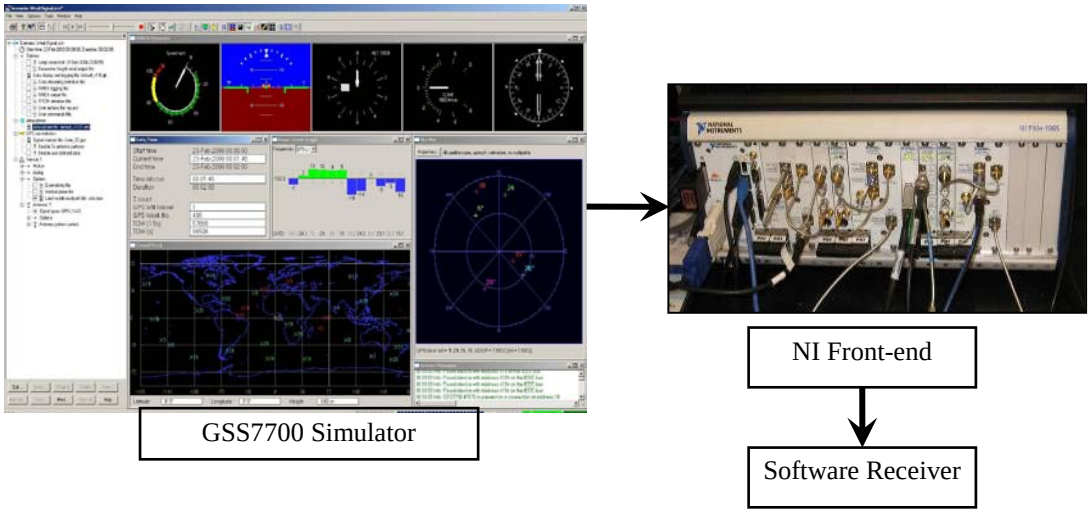

Fig. 4: Hardware setup

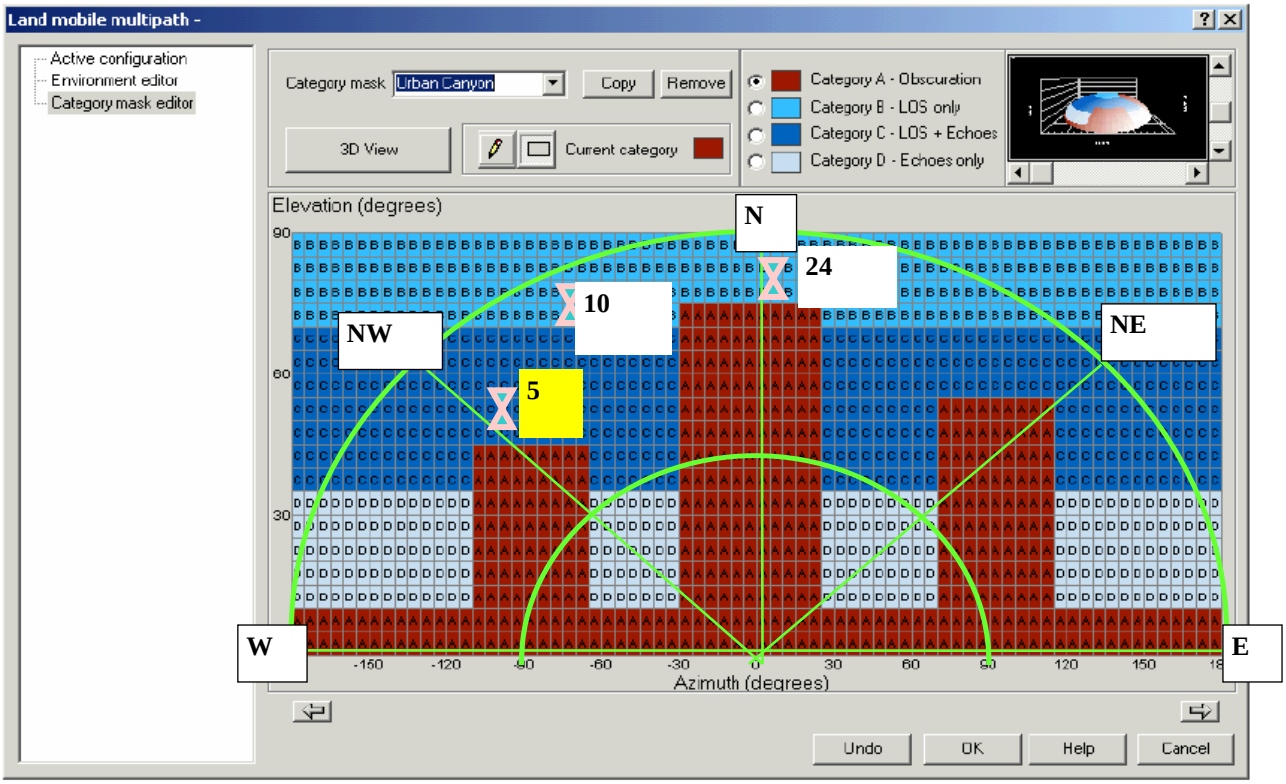

Fig. 5: multipath categories and satellites in view

Test B: Dynamic Vehicle

- Dynamic vehicle, with a velocity ranging between 25 km/hr and 100 km/hr, moving in a rectangular path shown in Fig. 6. The lower speed is used in turning, where the higher speed is used in the straight path. The acceleration from the low speed to the high speed is done within a distance of 100 m, with a constant acceleration of 4.3 m/s^2.
- Moderate signal power levels (The received L1 C/N_0 is 36 dB-Hz, and the L5 pilot C/N_0 is 39 dB-Hz).

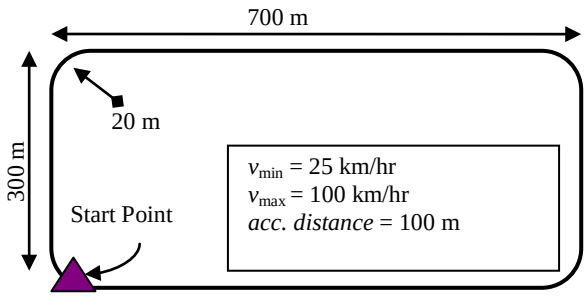

Fig. 6: Dynamic vehicle model

4.2 Results

In order to evaluate any signal tracking performance, the lock indicators are used. These lock indicators do not require the knowledge of the true tracking error. They are implemented to determine code, phase or frequency lock. The phase and frequency lock indicators inherently contain the code lock information.

The phase lock can be detected using the normalized estimate of the cosine of twice the carrier phase. The values of the lock indicator will range from -1, where the locally generated signal is completely out of phase with the incoming signal, and 1 that indicates perfect match.

The frequency lock can be determined using two consecutive samples of both the in-phase and quadrature correlator outputs. Similar to the PLI, the values of this lock indicator ranges from -1 to 1. Note that both indicators are often averaged to reduce their variances.

The results shown in this section are categorized into:

- The tracking performance analyzed by the phase lock indicators, the frequency lock indicators, the Doppler frequency and the correlator outputs of both frequencies using each of the two methods under comparison.
- The Kalman filter states and their corresponding standard deviations, for each of the two filters.

TEST A: Urban Canyon Multipath

1) Tracking errors:

Looking into the tracking errors in the urban multipath case, Fig. 7 shows the frequency lock indicator of the L1 frequency both for the separate Kalman filter case and for the combined Kalman filter case.

The combined Kalman filter has helped in enhancing the FLI in the urban canyon multipath environment and that is reflected in the less noise Doppler frequency estimate shown in Fig. 8.

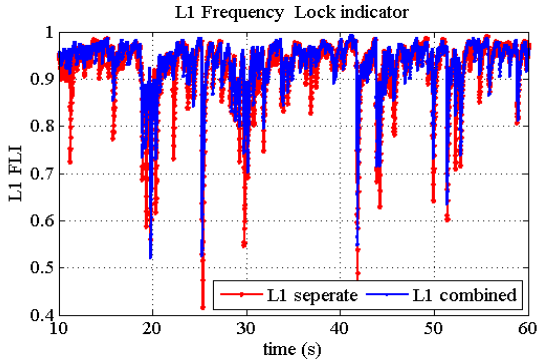

Fig. 7: L1 Frequency Lock Indicator

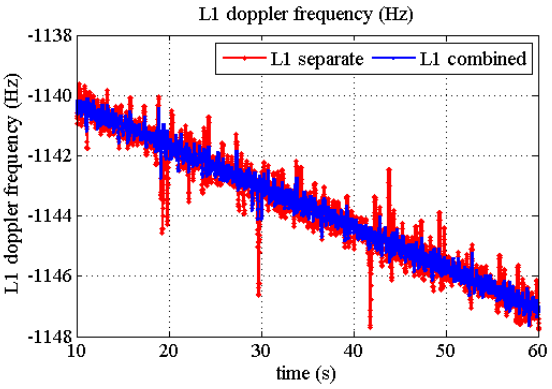

Fig. 8: L1 Doppler frequency

Fig. 9 zooms on the phase lock indicator of L1 in an interval where it suffers more power variations, and the corresponding correlator outputs are shown in Fig. 10. Though both the separate and the combined Kalman filter follow almost the same trend in both the PLI and the correlator output plots, Fig. 10 shows that the separate Kalman filter failed to maintain the phase lock and suffered a half-cycle slip as presented by the black and the green lines.

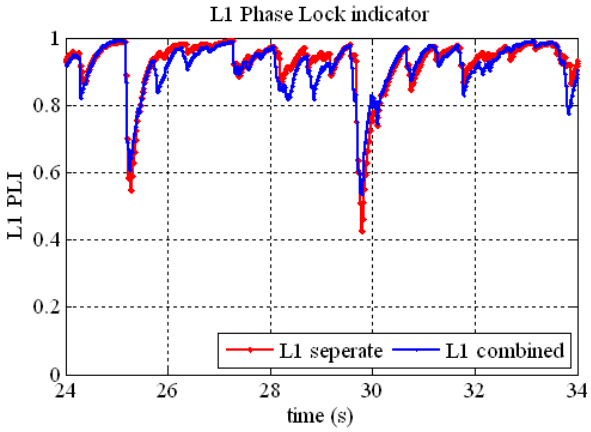

Fig. 9: L1 Phase Lock Indicator

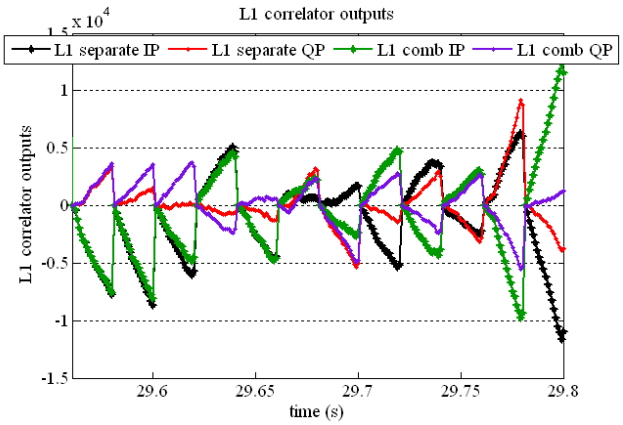

Fig. 10: L1 correlator outputs

On the other hand, the L5 pilot signal shows similar results when comparing both the separate and combined Kalman filter. Fig. 11 shows the PLI zoomed in the interval of higher signal variations, and the corresponding correlator outputs in Fig. 12. The combined Kalman filter clearly helps in decreasing the level of noise in the PLI and the correlator outputs.

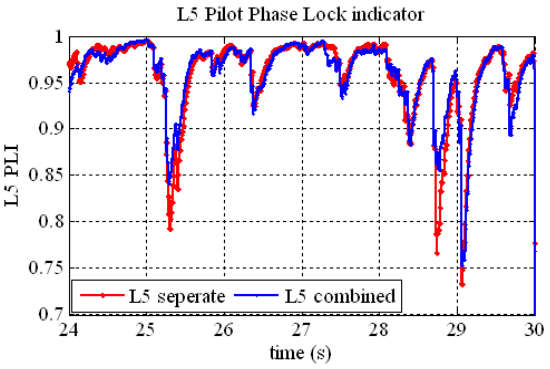

Fig. 11: L5 Pilot Phase Lock Indicator

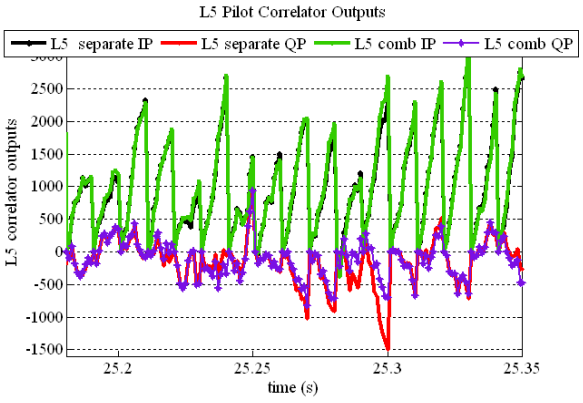

Fig. 12: L5 Pilot correlator outputs

2) Kalman filters Analysis:

The second category of results for this test is the Kalman filters states analysis. Since the main focus is on the carrier phase estimates, Fig. 13 shows the RMS of the carrier phase error, for both the L1 and L5 signals. The L1 signal shows decreased RMS error when using the combined Kalman filter with the pilot channel only, compared to the separate case.

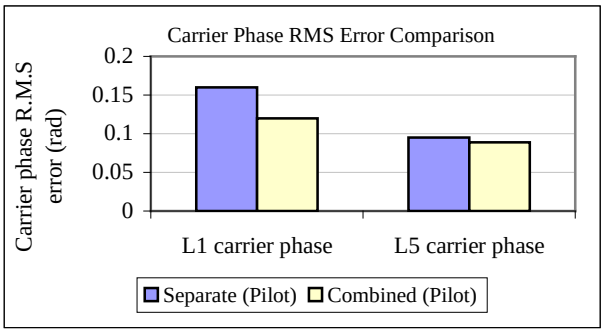

Fig. 13: Carrier phase RMS error comparison for urban canyon multipath scenario

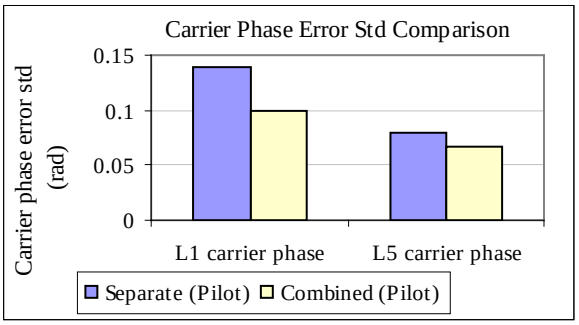

Fig. 14: Carrier phase error standard deviations comparison for urban canyon multipath scenario

On the other hand, for the L5 signal, the separate Kalman filter tracking shows better carrier phase error performance when compared with the combined Kalman filter tracking using the pilot channel only. The results are confirmed with the standard deviations shown in Fig. 14.

To further clarify the improvements when using the combined Kalman filter, Table IV summarizes the root mean square and the standard deviations of each of the estimated states in both cases and the corresponding improvements in percentile.

Table IV: Kalman filters statistics & improvements- Urban Canyon Multipath			
State		R.M.S	Average Std
$\delta\tau_s$ (chips)	L1 separate	0.00029	0.0022
	L1 combined	0.00026	0.002
	Improvement	10.3	9
	L5 separate	0.0042	0.0015
	L5 combined	0.0035	0.0014
	Improvement	16.6	6.6
$\delta\phi_s$ (rad)	L1 separate	0.16	0.14
	L1 combined	0.1	0.07
	Improvement	37.5	50
	L5 separate	0.064	0.03
	L5 combined	0.063	0.03
	Improvement	1.5	0
δf_s (Hz)	L5 separate	0.13	0.1
	L5 combined	0.128	0.1
	Improvement	1.5	0

TEST B: Dynamic Vehicle

1) Tracking errors:

The second test conducted is the dynamic user. The same sets of results are shown. Fig. 15 first shows the Doppler frequencies of both the L1 and the pilot L5 using the two kinds of filters. The separate and the combined Kalman filters both succeeded in tracking the signals under the tested velocity and acceleration. Note that the difference in the thickness is for illustration purpose only, not to indicate any difference in noise levels.

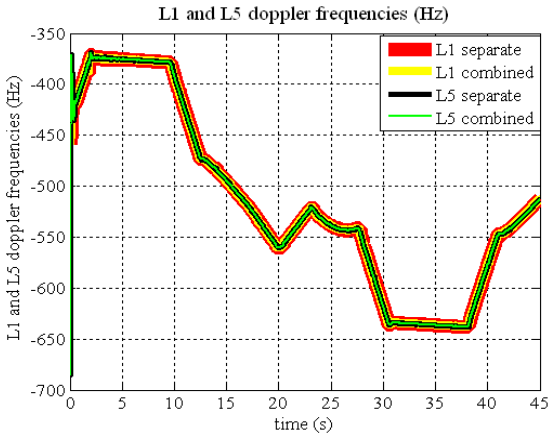

Fig. 15: L1 and L5 Doppler frequencies

By further examining the frequency and the phase lock indicators for the L1 signal in Fig. 16 and Fig. 17, it becomes clear that there is a big advantage from using the combined Kalman filter in the dynamic user case. The two indicators become higher and less noisy in the combined Kalman filter case.

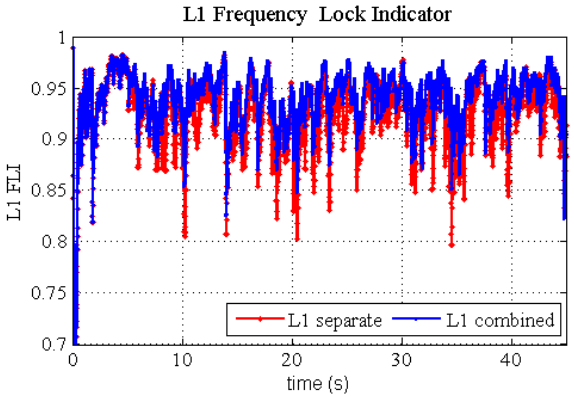

Fig. 16: L1 Frequency Lock Indicator

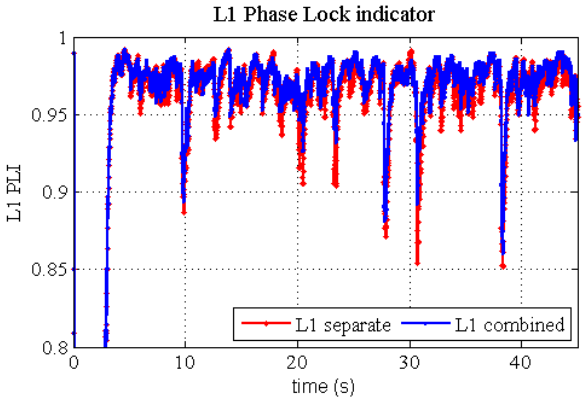

Fig. 17: L1 Phase lock Indicator

Similarly, for the L5 signal Fig. 18 and Fig. 19, the combined Kalman filter again shows much higher phase and frequency lock indicators when compared to the separate case.

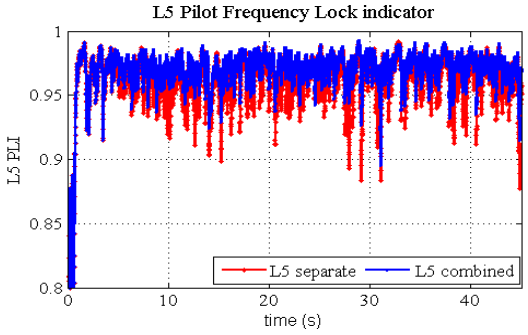

Fig. 18: L5 pilot frequency lock indicator

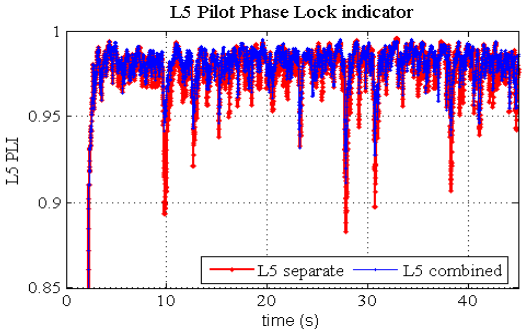

Fig. 19: L5 pilot phase lock indicator

2) Kalman filters Analysis:

Proceeding to the Kalman filter states analysis, Fig. 20 shows the RMS of the carrier phase error, for both the L1 and L5 signals. The L1 signal exhibits the least RMS errors when using the combined Kalman filter with both data and pilot channels. Contrary to the multipath case where the L1 estimates were noisy, the L5 signal is now making use of the L1 signal. This can be seen as thecombined Kalman filter with both the data and pilot channels yields lower carrier phase error compared to the separate case, using also both the data and pilot channels. The results are confirmed with the standard deviations shown in Fig. 21.

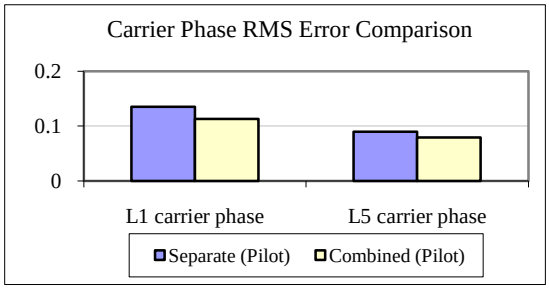

Fig. 20: Carrier phase RMS error comparison for moving vehicle scenario

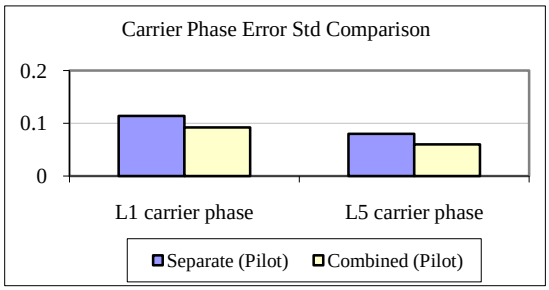

Fig. 21: Carrier phase error standard deviations comparison for moving vehicle scenario

Table V summarizes the statistics of the estimated states in both the separate and the combined Kalman filters with the corresponding improvements in percentile. Note that in case of the L1 code phase error, there is actually degradation in the rms calculated, but that is because both values are actually very low.

Table V: Kalman filters statistics & improvements- Dynamic Vehicle

State		R.M.S	Average Std
$\delta\tau_s$ (chips)	L1 separate	0.0004	0.002
	L1 combined	0.0005	0.002
	Improvement	-25	0
	L5 separate	0.0005	0.0026
	L5 combined	0.0004	0.0024
	Improvement	20	1.85
$\delta\phi_s$ (rad)	L1 separate	0.135	0.114
	L1 combined	0.113	0.092
	Improvement	16.3	4.4
	L5 separate	0.09	0.08
	L5 combined	0.079	0.06
	Improvement	12.2	4.3
δf_s (Hz)	L5 separate	0.28	0.183
	L5 combined	0.27	0.154
	Improvement	3.5	3.53

5 CONCLUSIONS

The paper shows a detailed performance analysis and comparison of the combined Kalman filter tracking, developed by Megahed et al (2009), versus the standalone Kalman filter. The environments under consideration included an urban canyon multipath environment that is a challenging environment for any tracking technique, and moderate ionospheric activity. The user model under consideration included typical vehicular acceleration levels and abrupt changes in direction. Both models were simulated using the Spirent GSS7700 signal simulator that provides a completely controllable environment to fully test the proposed tracking algorithms.

An extensive analysis of the tracking errors was conducted by examining the phase lock indicators, the frequency lock indicators, and the correlator outputs of

the L1 and the L5 signals under the two methods of comparison. Another set of analysis was conducted on the Kalman filter state estimates and the estimated standard deviations, and improvements were shown for each of the two signals.

Results show that the combined Kalman filter outperforms the separate Kalman filter in the tests conducted. Moreover, being a completely equivalent tracking method, it is safe to say that the combined Kalman filter outperforms the standalone Kalman filter and is worth to be used in under different conditions that involve user motion, moderate ionospheric errors or multipath environments.

Thus far, the combination of two signals has been beneficial in different environments. However, work presented in this paper has utilized only two (L5 pilot, L1) out of the three available channels (L5 data, L5 pilot and L1). More research should be done to investigate the feasibility, the advantages and the disadvantages of using also the L5 data channel and associated complexities.

Acknowledgments

The financial support of General Motors of Canada, the Natural Science and Engineering Research Council of Canada, Alberta Advanced Education and Technology and the Western Economic Diversification Canada is acknowledged.

References

IS-GPS-2006 (2006), ***Interface Specification – Navstar GPS Space Segment/ Navigation User Interfaces***, ARINC Incorporated, March 2006.

Braasch M., S. Gunawardena and Z. Zhu (2009), *First Look: **Observing the GPS L5 Test Transmission from SVN49 Using Software Radio Processing***, Inside GNSS, Technical article, May/June 2009.

Hu, T., G. Lachapelle and R. Klukas (2005) ,***Indoor GPS Signal Replication Using a Hardware Simulator***, in Proceedings of ION GNSS 2005, Long Beach, CA, September 13-16, 2005.

Inside GNSS (2009), ***GPS Satellite with L5 Payload Launches Successful***, 24 March 2009.

Megahed, D., C. O'Driscoll, and G. Lachapelle (2009), ***Combined L1/L5 Kalman Filter-Based Tracking for Weak Signal Environments***, in the proceedings of the European Navigation Conference - Global Navigation Satellite Systems, ENC-GNSS 2009, Naples, Italy, May 2009.

Meurer, M., S. Erker, S. Thölert, O. Montenbruck, A. Hauschild and R. B. Langley (2009) ***Innovation: L5 Signal First Light, A Preliminary Analysis of SVN49's Demonstration Signal***, in GPS World, June 1, 2009.

Mongrédien, C., G. Lachapelle, and M. E. Cannon (2006), ***Testing GPS L5 Acquisition and Tracking Algorithms Using a Hardware Simulator***, in Proceedings of ION GNSS 2006, 26-29 September, pp. 2901-2913, Fort Worth, TX.

Mongrédien, C., G. Lachapelle and M.E. Cannon (2008), ***Testing GPS L5 Tracking Algorithms and their Impact on Positioning Accuracy***, in Proceedings of European Navigation Conference (Toulouse, 23-25 April), 10 pages.

Lachapelle, G., E. Cannon, R. Klukas, S. Singh, R. Watson P. Boulton, A. Read and K. Jones (2003), ***Hardware Simulator Models and Methodologies for Controlled Indoor Performance Assessment of High Sensitivity AGPS Receivers***, in Proceedings of GNSS 2003, Graz, Australia, 22-25 April 2003.

Petovello, M.G. and G. Lachapelle (2006), ***Comparison of Vector-Based Software Receiver Implementation with Applications to Ultra-Tight GPS/INS Integration***, in roceedings of ION GNSS 2006.

Psiaki, M.L. and H. Jung (2002), ***Extended Kalman Filter Methods for Tracking Weak GPS Signals***, in Proceedings of ION GPS 2002.

Spirent (2006), ***Signal Generator Hardware User Manual, Spirent Communications***, issue 1-20, September 2006.

Ward, P. W., J. W. Betz, and C. J. Hegarty (2006), *Satellite **Signal Acquisition, Tracking and Data Demodulation***, in Understanding GPS Principles and Applications, second edition , Artech House Mobile Communications Series, p. 153.

BIOGRAPHY

Dina Reda Salem is a PhD candidate in the Position, Location And Navigation (PLAN) group at the Geomatics Engineering Department in the University of Calgary. She received both her bachelor and masters degrees in Electrical Communications from Cairo University in Egypt. Her current research focuses on GNSS software receiver design for weak signal Tracking.